Interpretation of Electron Channeling by the Dynamical Theory of Electron Diffraction

K. Kambe, G. Lehmpfuhl, and F. Fujimoto *

Fritz-Haber-Institut der Max-Planck-Gesellschaft, Berlin
* College of General Education, University of Tokyo, Tokyo 153, Japan

The connection between electron channeling and electron diffraction is discussed on the basis of the dynamical theory. Results of the many-beam calculations for 50 keV to 2 MeV electrons incident almost parallel to a [110] axis of a MgO crystal are used as examples. Bloch waves with a marked concentration of electron density at rows of atoms are obtained, and interpreted as states of electrons bound to the rows of atoms, corresponding to the classical picture of channeling. This can be shown properly by applying the tight-binding method of band theory in the two dimensions perpendicular to the axis. In this picture the "rosette motions" in the classical theory are interpreted as p-type, d-type, etc. Bloch waves, and the "weavons" as loosely-bound s-type Bloch waves. They are connected to the pictures of the Borrmann effect and the Bloch-wave channeling in the diffraction theory.

Electron channeling takes a particular position among the channeling effects in the motion of high-energy particles through crystals (cf. Gemmel [1], Chap. 5, Chadderton [2]). Contrary to positively charged particles the scattering intensity in higher angles (Rutherford scattering) is expected to *increase* for electrons moving parallel to a zone axis or netplane. Actually, an intensity maximum has been observed in the Rutherford scattering when the incident beam is parallel to a zone axis [3].

Correspondingly, an intensity minimum is expected for the forward scattering (transmitted beam). Kreiner et al. [4, 5] found, however, a peak inside a broad dip of the transmitted beam, and proposed as its interpretation the effect of "rosette motion" of electrons around the rows of atoms. Nip et al. [6] have proposed a "weavon" model for the explanation of the maximum. Discussions comparing the two models were given by Kumm et al. [5] and Nip et al. [7].

Taking advantage of the reciprocity principle ("reversibility" of Lindhard [8]) Fujimoto et al. [9] have studied electron channeling by observing Kikuchi patterns, which are interpreted usually in terms of electron diffraction. They pointed out that in the Kikuchi patterns obtained in the higher-angle scattering (Rutherford scattering) one always finds around a zone axis an intensity maximum as an average over diffraction contrasts.

Concerning the problem whether we get a peak or a dip in the transmitted beam, a series of new pictures have been taken by Fujimoto et al. [10] by using various improved techniques of electron diffraction and electron microscopy. These pictures show intensity peaks distributed characteristically inside an average dip around a zone-axis direction, revealing that the situation is somewhat complicated.

Quite recently, Bobudaev et al. [11] observed two peaks inside a broad dip of the transmitted beam, and explained them by the rosette motion picture [4, 5].

The relation between electron diffraction and electron channeling has been studied by several authors (cf. Ref. 1, 2). Their theory is based on the Bloch-wave formalism of the dynamical theory of electron diffraction [12, 13], and they have attempted to connect the channeling effect to the so-called many-beam effect and anomalous absorption. However, the essential physical picture has been clarified quite recently by Berry et al. [14]. On the basis of a semiclassical theory of electron diffraction [15, 16] they show that classical channeling trajectories can be interpreted as "bound Bloch waves" in the wave theory.

In the present paper we intend to clarify the nature of electron channeling, particularly of the rosette motion, in terms of the bound-Bloch-wave picture. The basis of the discussion is the discovery [17, 18] of the bound-Bloch-waves in the analysis of diffraction patterns from MgO crystals and their interpretation by means of a tight-binding approach to the dynamical theory of electron diffraction [19].

The basic ideas are given already in the preliminary report [10].

§ 1. Electron-Density Distribution of Bloch Waves

In the analysis of electron-diffraction patterns obtained by transmission through wedge-shaped crystals the electron-density distribution was calculated for each Bloch wave [17]. The Bloch waves were derived by the usual many-beam calculation of the dynamical theory.

In the typical cases of MgO, when the direction of the primary beam at 50 keV is nearly parallel to the zone axis [$\bar{1}$10] (Fig. 1), it has been found that the density distribution of two strongly excited Bloch waves is markedly concentrated at the positions of the rows of Mg and O atoms respectively. The third Bloch wave has zeroes of density at the centers of the rows of atoms, and maxima between the rows.

In the usual picture of the dynamical theory [12, 13] the first two Bloch waves are those for which the "beat" between the component plane waves show the maxima at the positions of atomic rows. The marked sharpness of the peak is understood as a many-beam effect [13]. The third Bloch wave has the nodes at the positions of atomic rows, contributing to an anomalously enhanced total transmission (Borrmann effect, cf. Ref. 12, p. 204).

On the other hand, as already pointed out [17] the first two Bloch waves, which are apparently *bound* to the rows of atoms, can be interpreted as the wave-

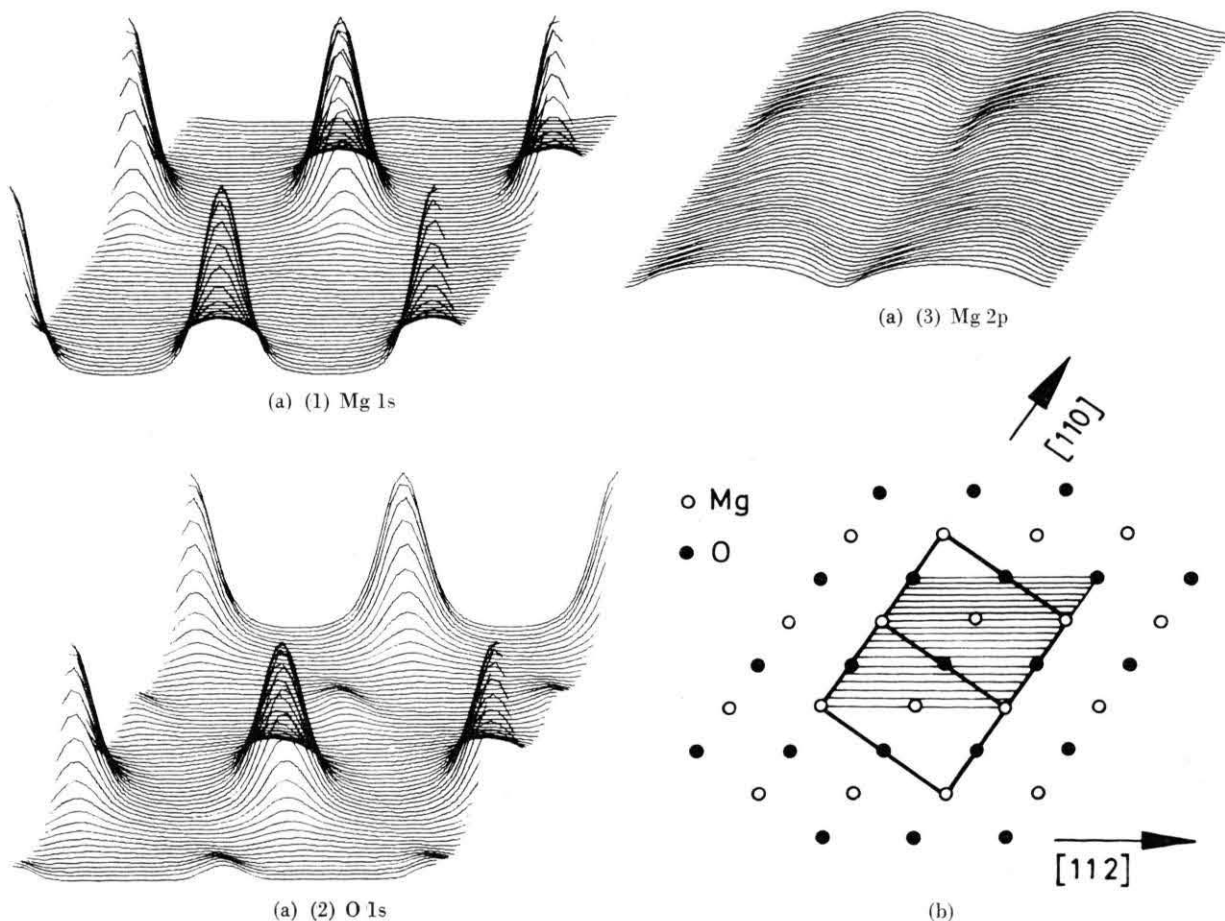Fig. 1. (a) Electron density distribution of Bloch waves. Results of the dynamical 42 ∼ 43 beam calculations. 50 keV electrons. MgO[$\bar{1}$10] axis. Bragg position for (002) reflection at [001] azimuth. The Bloch waves are normalized to unit average density. The densities are in an arbitrary scale. The Bloch waves are numbered in the sequence of increasing transverse energy. (b) The area of the density maps.

mechanical counterpart of the channeling of electrons in the classical particle picture (Lindhard [8]), the paths of electrons being localized at minima of the crystal potential, that is, at the rows of atoms. This interpretation has been supported by the test calculations for positrons [17], the Bloch waves of which have shown a localization of density again at the potential minima, that is, in this case *between* the rows of atoms.

In the present paper we are concerned particularly with the third Bloch wave of electrons, which has zero density at the centers of atomic rows. As already pointed out [10] this Bloch wave may be interpreted as the wave-mechanical counterpart of the rosette motion.

This interpretation becomes more obvious in the calculations similar to Fig. 1 for higher energies of electrons [18]. The conditions of calculation are exactly the same as those for 50 keV [17]. Only the electron energy is increased. The number of beams (42 − 43) used in the calculation is obviously too small for getting a quantitatively reliable result, but believed to be large enough for a qualitative discussion.

As shown in Fig. 2 at 1 MeV we see clearly that the Bloch waves 3 and 4 are also localized in the neighbourhood of the rows of atoms, showing a pair of maxima around the center. This indicates that at 1 MeV these Bloch waves are also "bound" to the atomic rows. At 2 MeV as shown in Fig. 3 more Bloch waves are found to be bound.
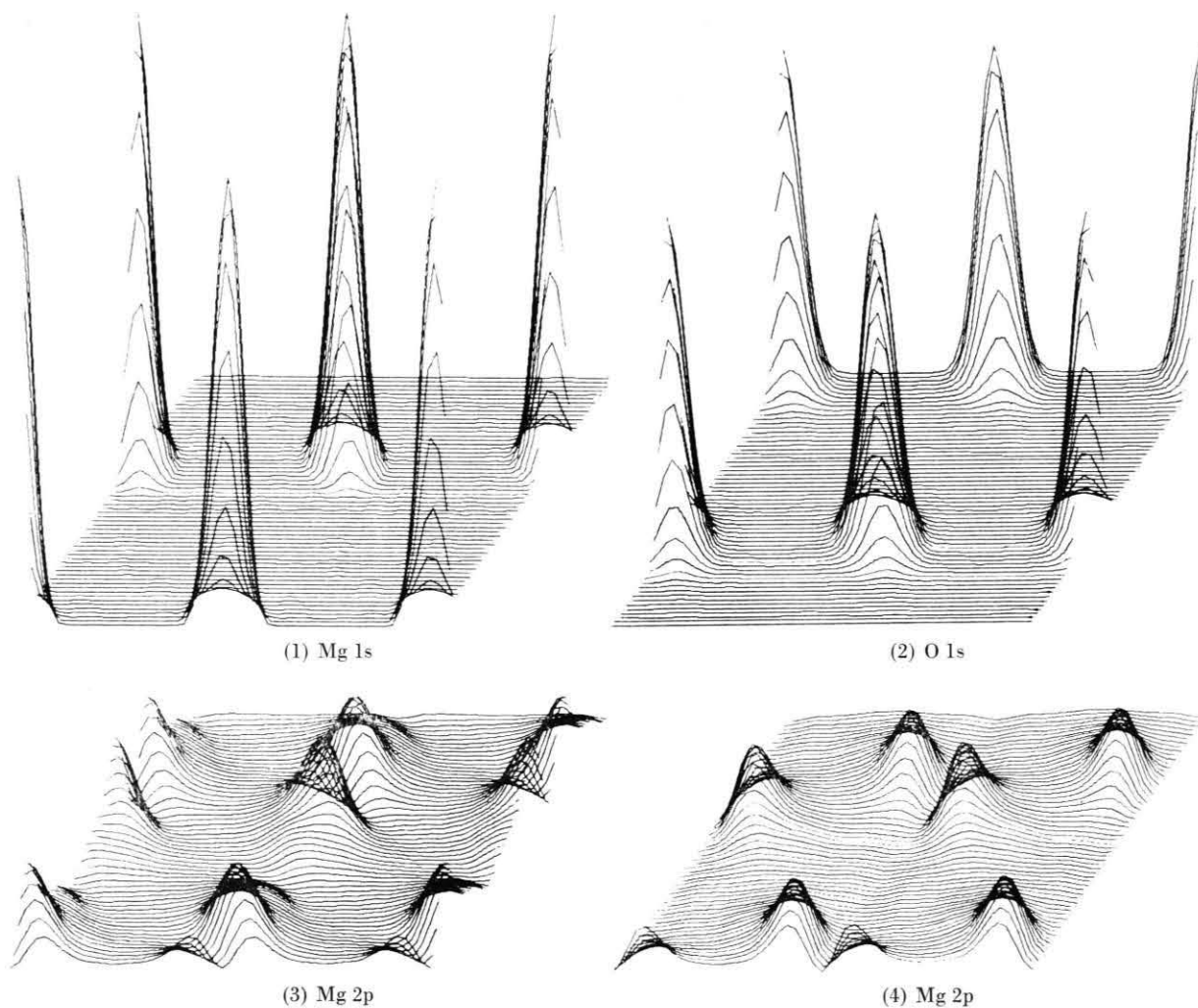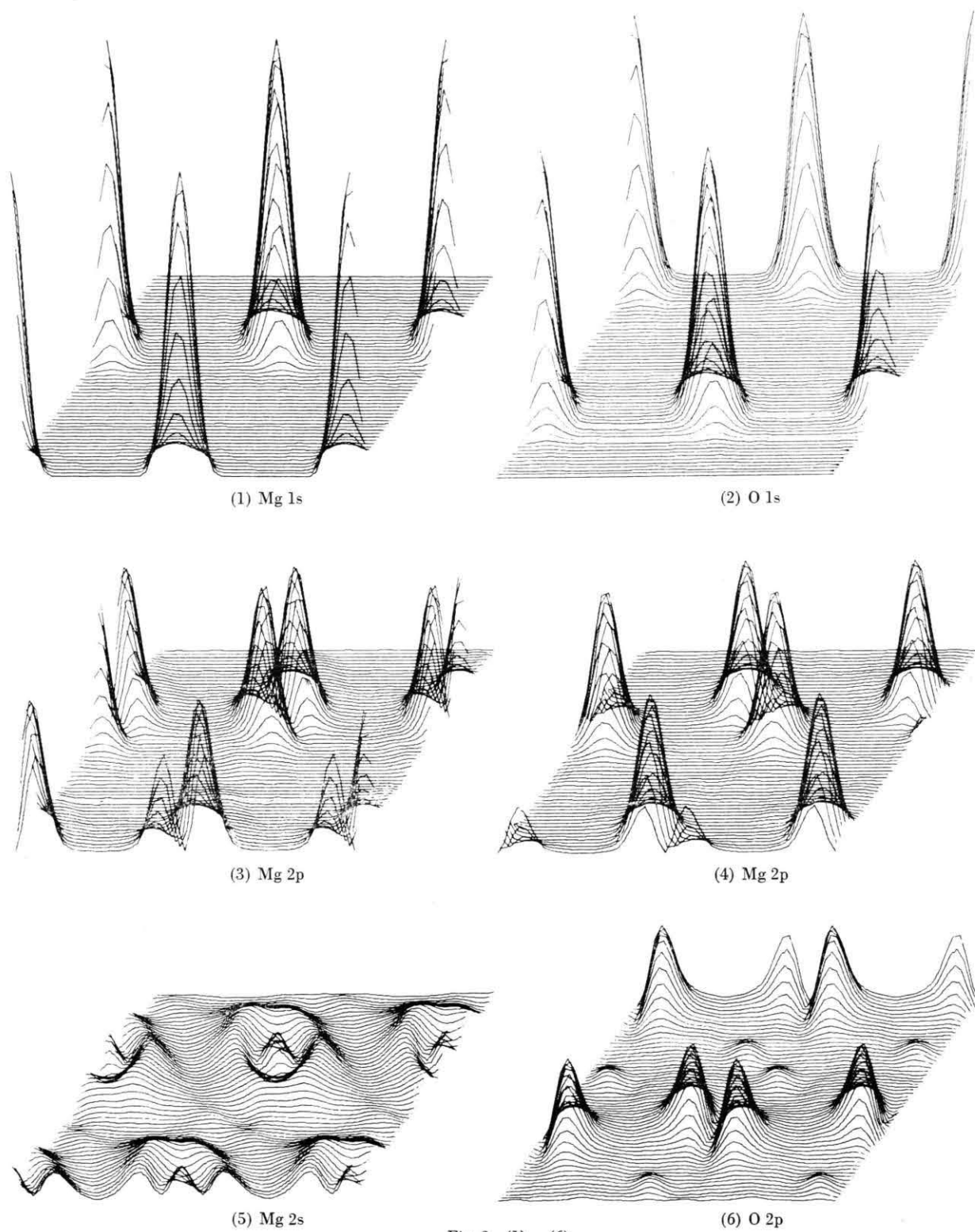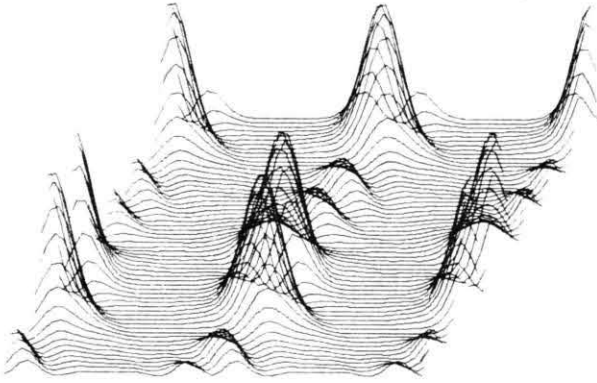

(1) Mg 1s

(2) O 1s

(3) Mg 2p

(4) Mg 2p

Fig. 2. Same as Fig. 1: 1 MeV electrons. Bloch wave 3 is not excited but included here to show that the p-type Bloch waves exist always pairwise.

(1) Mg 1s

(2) O 1s

(3) Mg 2p

(4) Mg 2p

(5) Mg 2s

(6) O 2p

Fig. 3. (1) — (6)

(7) O 2p

Fig. 3. Same as Fig. 1: 2 MeV electrons. Bloch waves 3 and 7 are not excited.

§ 2. Tight-Binding Formalism

It is obvious that this kind of bound Bloch waves can best be interpreted by means of the "tight-binding method" known in band theory of solid states. By "tight binding" it is implied, of course, only in the two dimensions perpendicular to the zone axis. The movement of electrons is still "nearly free" in the direction parallel to the axis. The details of formalism will be given in a separate paper [19]. Here we recapitulate only a few essential points which are immediately necessary for our discussion.

It is assumed, for simplicity, that the entrance surface of the crystal is perpendicular to the zone axis (z-axis). Then the solution inside the crystal is given by

$$\psi(x,y,z) = \sum_i a^{(i)}(K_{0x}, K_{0y}) \psi^{(i)}(x,y,z), \quad (1)$$

where $\psi^{(i)}(x,y,z)$ are Bloch waves normalized in a unit cell. Their amplitudes $a^{(i)}(K_{0x}, K_{0y})$ are determined from the boundary conditions at the entrance surface. K_{0x} and K_{0y} are the tangential components of the wave-vector of the incident electrons, and the tangential components k_x and k_y of the wave-vectors of all the Bloch waves should be equal to them respectively. We call $a^{(i)}$ the "excitation amplitudes" of Bloch waves, and $|a^{(i)}|^2$ the "excitation strengths".

In the approximation where only the "zero-order Laue zone" (cf. Hirsch et al. [12], p. 112) is taken into account, the variation of the potential parallel to the zone axis is neglected, corresponding to the "continuum approximation" of Lindhard [8]. In this case we can show easily that the i-th Bloch wave is written in the form

$$\psi^{(i)}(x,y,z) = \varphi^{(i)}(x,y) \exp\{i k_z^{(i)} z\}, \quad (2)$$

where the function $\varphi^{(i)}(x,y)$ satisfies

$$\frac{d^2\varphi^{(i)}}{dx^2} + \frac{d^2\varphi^{(i)}}{dy^2} + \frac{2m}{\hbar^2}(E_t^{(i)} - V(x,y))\varphi^{(i)} = 0, \quad (3)$$

with $E_t^{(i)}$ the "transverse energy" [8], m the relativistic mass of the incident electron

$$m = m_0(1 + E/(m_0 c^2)). \quad (4)$$

E is the kinetic energy of the incident electron in vacuum. $V(x,y)$ is the "continuum potential" [8], the average of the crystal potential along the z-direction.

Regarding $E_t^{(i)}$ as a function of the wave-vector components k_x and k_y, Eq. (3) represents an energy-band problem in the two-dimensional space. $E_t^{(i)}$ is the i-th eigenvalue of the transverse energy and $\varphi^{(i)}$ the corresponding eigenfunction.

The value of $k_z^{(i)}$ in Eq. (2) is determined from the value of $E_t^{(i)}$ by

$$k_z^{(i)2} = \frac{2m_0}{\hbar^2} E\left(1 + \frac{E}{2m_0 c^2}\right) - \frac{2m}{\hbar^2} E_t^{(i)}. \quad (5)$$

In the usual dynamical theory [12, 13] $k_z^{(i)}$ as a function of k_x and k_y constructs a branch of "dispersion surface" in the reciprocal space.

In the standard many-beam calculations [12, 13] the Bloch wave $\psi^{(i)}$ given by Eq. (2) is expanded into plane waves. This means that the function $\varphi^{(i)}$ is written in the form

$$\varphi^{(i)}(x,y) = \sum_g c_g^{(i)}(k_x, k_y) \exp\{i(k_x + 2\pi g_x)x \\ + i(k_y + 2\pi g_y)y\}, \quad (6)$$

where the summation is taken over the two-dimensional reciprocal lattice points. g_x and g_y are the components of the reciprocal lattice vectors. $c_g^{(i)}(k_x, k_y)$ are the plane-wave amplitudes which are determined by substituting Eq. (6) into Equation (3). All the numerical results shown in the present paper are obtained by this method. In the terminology of band theory this method is called the nearly-free-electron approach.

In the tight-binding approach [19] the solution $\varphi^{(i)}(x,y)$ is written in the form

$$\varphi^{(i)}(x,y) = \sum_m \sum_n c_{mn}^{(i)} \chi_{mn}(x - x_m, y - y_m), \quad (7)$$

where

$$\chi_{mn}(x,y) = \sum_{n_1} \sum_{n_2} u_{mn}(x - n_1 a_1, y - n_2 a_2) \\ \cdot \exp\{i(k_x n_1 a_1 + k_y n_2 a_2)\}. \quad (8)$$

The function $u_{mn}(x, y)$ is the n-th bound state of the m-th string in the unit cell. The summations in Eq. (8), called the Bloch sum, are taken over the real lattice points, n_1 and n_2 being integers, a_1 and a_2 the lattice constants. For simplicity a rectangular lattice is assumed. The summations in Eq. (7) are taken over the strings m in a unit cell, x_m and y_m indicating the position of the string in a unit cell, and over the bound states n. $c_{mn}^{(i)}$ are constants which are derived by the variational method applied to the wave Equation (3).

The continuum potential $V(x, y)$, is assumed as the superposition of the "continuum string potentials"[8] $V_m(x, y)$, which is the average of atomic potentials for a single row, or "string"[8], of atoms. Thus,

$$V(x, y) = \sum_{n_1} \sum_{n_2} V_m (x - n_1 a_1, y - n_2 a_2) . \qquad (9)$$

Assuming that the string potential $V_m(x, y)$ has a circular symmetry around the string, we write in the polar coordinates r and φ

$$V_m(x, y) = V_m(r) , \qquad (10)$$

and

$$u_{mn}(x, y) = R_{mn}(r) \cos(l_n \varphi) \quad \text{or} \quad R_{mn}(r) \sin(l_n \varphi) , \qquad (11)$$

where $l_n = 0, 1, 2$, etc. is the angular quantum number of the n-th bound state.

The radial part $R_{mn}(r)$ satisfies

$$\frac{1}{r} \frac{d}{dr} \left(r \frac{dR_{mn}}{dr} \right) + \left(\frac{2m}{\hbar^2} [E_{mn} - V_m(r)] - \frac{l_n^2}{r^2} \right) R_{mn} = 0 . \qquad (12)$$

All these formulas are analogous to the usual three-dimensional problem of bound states in a central field. Accordingly, the bound states in two dimensions with $l_n = 0, 1, 2$, etc. are called the s-type, p-type, d-type, etc. states. In the following examples the Bloch waves contain effectively only one of these states, and are called in the same manner.

If a Bloch wave contains only one bound-state function u_{mn}, it can be shown[19] that the excitation amplitudes of the Bloch waves $a^{(i)}$ in Eq. (1) are given by

$$a^{(i)} (K_{0x}, K_{0y}) \qquad (13)$$
$$= \text{const} \int_{-\infty}^{\infty} dx \int_{-\infty}^{\infty} dy \, u_{mn}^*(x, y) \exp\{i(K_{0x} x + K_{0y} y)\},$$

where K_{0x} and K_{0y} are the components of the wave vector of the incident wave. Equation (13) has a form of the inner product between the incident plane wave and the bound-state function, implying physically that this part of the incident wave is going into the bound state. Mathematically, Eq. (13) is nothing but a Fourier transform.

§ 3. Interpretation of Bloch Waves by the Tight-Binding Picture

The Bloch waves 1 and 2 in Figs. 1, 2 and 3 are obviously the s-type states of Mg and O respectively. The Bloch waves 3 and 4 are the p-type states of Mg. This is seen clearly by the appearance of double maxima in Figs. 2 and 3. A wave-amplitude analysis shows also that for these two maxima the sign of the wave function is just opposite, as is expected for a p-type state. In Fig. 1 the p-type bound-state functions u_{mn} are strongly overlapped to each other, so that large maxima between the strings appear, loosing the double-peak character. The strong overlap indicates that this state is not bound. In fact, it is not appropriate to apply the tight-binding picture to this kind of "free Bloch waves".

In Fig. 3 a higher-order s-type bound state of Mg appears as Bloch wave 5, showing clearly a 2 s-type character with a ring of the node line of the wave function around the center. In this sense the Bloch waves 1 and 2 may be called 1 s-type, and Bloch waves 3 and 4 2 p-type and so on.

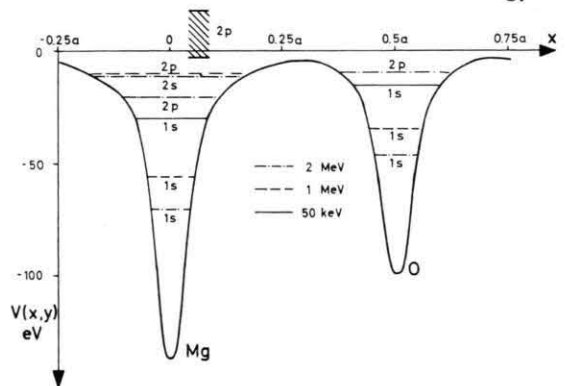Other higher-order states become successively bound with the increase of the electron energy E.

Fig. 4. Levels of transverse energy for Bloch waves. The broad band of Bloch wave 3 (Mg 2p) at 50 keV is a typical example of nearly-free states. The upper-lying bound levels are slightly broadened. The potential curve is the cross-section of the continuum potential $V(x, y)$ along the x-axis [001]. a = lattice constant 4.202 A.

This is due to the increase of the attractive potential term $(2 m/\hbar^2) V_m(r)$ in Eq. (12) with the relativistic increase of the electron mass m after Equation (4).

The boundness of the states is made visible also by a comparison of the level of transverse energy $E_t^{(i)}$ with the continuum potential $V(x, y)$ as shown in Figure 4. The levels for 50 keV, 1 MeV and 2 MeV electrons are put into the potential curve. It is seen that the levels of the bound states go down deeper into the potential wells of the strings with increasing energy of the primary electrons. Correspondingly, a stronger localization of the Bloch waves appear as shown in Figs. 1, 2 and 3.

The fact that these levels are really bound states of single strings has been proved separately by a numerical solution of Equation (12)[19].

§ 4. Interpretation of Rosette Motions

Since $l_n = 0$, the s-type states have no angular momentum around a string. This means that the corresponding projections of classical orbitals on the $x y$-plane should be straight line-segments going through the center of the string. Generally, this gives rise to an increased Rutherford scattering of electrons. The fact that these states *are* relatively strongly excited explains the average increase of Rutherford scattering of electrons moving in a zone-ais direction[3]. However, the weavons of Nip et al.[6] causing a *reduced* Rutherford scattering belong also to this type. They will be discussed in § 6.

On the other hand, the p-type states have a finite angular momentum, and correspond to rosette motions in the classical picture. Since rosette orbitals do not hit the center region of strings, provided that they are not too tightly bound, there is only a small Rutherford scattering[4, 5].

It is seen in this way that *the phenomenon of rosette motion is present not only at very high energies for which a classical picture is more proper, but also at 1 MeV and even at lower energies in the form of p-type bound-state Bloch waves.* In the example of Fig. 2 only one pair of such states is present at 1 MeV (Bloch wave 3 and 4) due to the quantum conditions for angular momentum and energy. A classical picture[4, 5] without any quantum condition is valid at very high energies of the primary electrons, at which a sufficiently large number of p-states, d-states, etc. are bound, each of which corresponding to a rosette motion. The opposite

limit is arrived at 50 keV, at which no rosette motion is allowed due to the quantum conditions. The strong overlap of the p-type states indicates that an electron in this state is nearly free (cf. Figure 4). It can easily go over from one string to another. Even though, the electron undergoes a small Rutherford scattering, since it does not hit the centers of strings. In this sence, the Bloch wave 3 in Fig. 1 showing maxima between the strings does not correspond directly to a rosette motion in the classical sense, but is closely related to it.

In general, the energy above which the p-type bound Bloch waves appear is determined approximately by the interaction parameter α_a defined by Fujimoto et al.[9].

§ 5. Angular Dependence of the Excitation of Rosette Motions

§§ 5.1. Tilt Angle

Since a rosette motion should have a non-vanishing angular momentum around a string, it can appear only if the incident beam is slightly tilted to the zone axis. It disappears again at higher tilt angles due to the decrease of the number of electrons having a proper value of angular momentum. Accordingly, a profile of the number of electrons going into rosette motions as a function of the tilt angle shows two peaks on the both sides of the exact axis direction (cf. Bobudaev et al.[11]). Fujimoto et al.[10] observed corresponding rings around the axis direction.

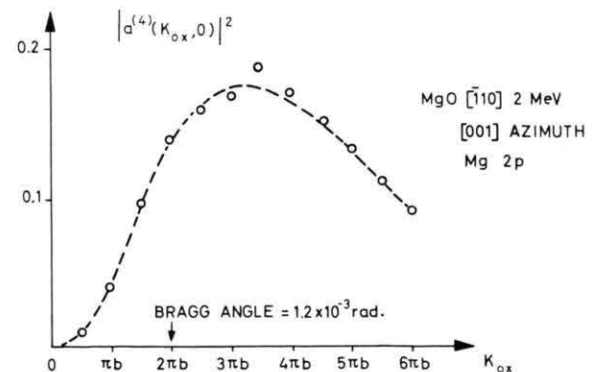A corresponding dependence of the excitation strength $|a^{(i)}|^2$ of the p-type Bloch wave on the tilt

Fig. 5. Excitation strength of the p-type Bloch wave at 2 MeV as a function of the tilt angle measured in K_{ox}, the x-component of the primary wave vector. $b = 1/a = 0.238$ Å^{-1}. The fluctuation of the calculated points is caused by the limitation of the number of beams in calculation.

angle has been found e. g. at 2 MeV as shown in Fig. 5 (Bloch wave 4, Figure 3). We find the same form as those of Bobudaev et al. [11]. This characteristic form is explained in terms of the tight-binding theory as the result of the Fourier-transform Equation (13).
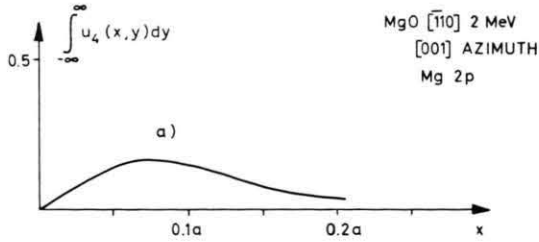

Fig. 6. (a) The projection of the fourth bound-state function (Mg 2p) on the x-axis. 2 MeV electrons.
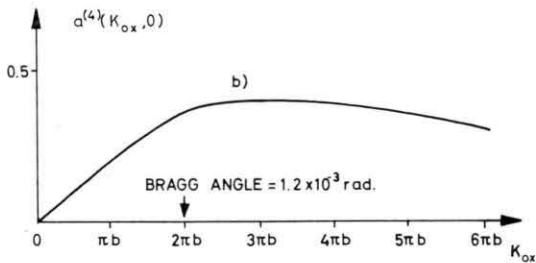

Fig. 6. (b) The corresponding excitation amplitude of the Bloch wave 4 on the k_x-axis.

Thus, Fig. 6(a) shows the function $\int u_{mn}(x,y)\,dy$, the projection of u_{mn} on the x-axis, obtained for the p-type Bloch wave at [001]. The corresponding excitation amplitude $a^{(i)}(K_{0x},0)$ is shown in Figure 6(b). The curve (a) was obtained for $K_{0x}=0$, whereas the curve (b) by a sequence of calculations for varying values of K_{0x}. It is seen directly that these two functions are approximately Fourier transforms to each other.

We note that in Fig. 6(b) the value of the excitation amplitude $a^{(i)}(K_{0x},0)$ varies slowly over several multiples of the Bragg angle, being the Fourier transform of a strongly localized bound-state function, which covers only one fifth of the lattice period (Figure 6(a)). This is a general characteristic of a "bound Bloch wave", showing again its close connection to the channeling effect.

§§ 5.2. Azimuthal Angle

If the string potential had a circular symmetry, the rosette motion in the classical picture would have also a circular symmetry. It is expected that the excitation of the rosette motion would be independent of the azimuthal direction of the primary beam. In reality the potential around a string has a deviation from circular symmetry due to the surrounding strings, so that the excitation strength of rosette motion should vary with the azimuthal angle. This effect is expected to be more pronounced for the states with higher transverse energies, for which the rosette orbitals are more extended around a string.

The corresponding dependence of the excitation of p-type Bloch waves on the azimuthal angle is somewhat complicated. If the string potential had a circular symmetry, we know from Eq. (11) that there would be two degenerate p-type states for each string, as shown approximately in Figs. 2 and 3. Any linear combination of these two states would be a possible state, and only that state which has a mirror symmetry with respect to the left-and-right of the incident beam would be excited. (In the example of Fig. 2 at the azimuth [001] Bloch wave 3 is not excited.) The excitation amplitude would not vary with the azimuthal angle. This would correspond to a circular symmetry of the rosette motion.

A deviation from this circular symmetry due to the surrounding strings can be introduced in two ways. The first is the deformation of the bound state itself due to the overlap of the string potentials. The second is the overlap of the bound-state wavefunctions between the strings, as seen in Fig. 1 at 50 keV. Both can give rise to a removal of the degeneracy of two p-type states. There are two *nearly* p-type states as new eigenfunctions with corresponding two Bloch waves. The typical examples are Bloch waves 3 and 4 in Figure 2. The sum of excitation strengths $|a^{(i)}|^2$ of these two Bloch waves may be regarded as a new *total* excitation strength of the p-type states under consideration.

Figure 7 shows the total excitation strength of the p-type Bloch waves at 2 MeV corresponding to the ones in Fig. 3 as a function of the azimuthal angle of the primary beam. The difference between the two curves can be understood by the difference in energy levels shown in Figure 4. We see clearly that the 2 p-type Bloch waves of Mg having deeper-lying levels show a much less azimuth dependence than those of O.

At any case it appears that a reasonable physical interpretation of the dependence on the azimuthal angle cannot be given without going into the details of the overlap between the bound-state functions.
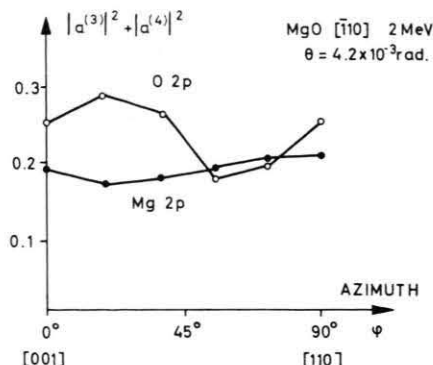
Fig. 7. Total excitation strength of the p-type Bloch waves for Mg and O as a function of the azimuthal angle of the primary beam. The tilt angle $(4.2 \times 10^{-3}$ rad) corresponds to $\sqrt{K_{0x}^2 + K_{0y}^2} = 3.5 \, \pi \, b$.

§§ 5.3. Discussion of Angular Dependence

The examples of MgO indicate that the considerations given above can be applied also to the observations of characteristic intensity distribution around a zone axis in electron diffraction and microscopy [10] as mentioned in the introduction. However, the Fourier transform concept of Eq. (13) predicts immediately that strongly localized bound states at lower levels of transverse energy can contribute only to a gradual change of the intensity, as we have seen in Figure 5. They may contribute mainly to the *average* increase (s-type) or decrease (p-type etc.) of the Rutherford scattering around a zone-axis direction, depending on the values of related physical parameters (cf. § 7). The sharp-contrasted figures observed [10], such as spots, rings, streaks, etc., can only be caused by uppermost bound states and/or free states, to which a more detailed analysis of overlap is necessary. We have just seen above, in the examples of Fig. 7, that the effect of overlap is apparently important for interpreting such kind of intensity variations.

§ 6. The Planar Cases and the Bloch-Wave Channeling

When the direction of the primary beam is nearly parallel to one of the main lattice-planes of a crystal and not to any zone axis, we have a "planar" channeling case. In the terminology of electron diffraction this is a "systematic" case, in which only the reciprocal points lying on one reciprocal rod are taken into account. In this case we have a one-dimensionally periodic potential, which is regarded as constant in directions parallel to the lattice plane (Figure 8 a).
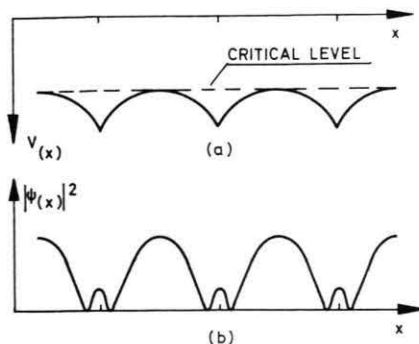

Fig. 8. **Planar case with systematic many-beam interactions.** (a) Planar average potential $V(x)$ and the critical level of transverse energy. (b) Schematic density distribution of the Bloch wave at the critical level leading to the Bloch-wave channeling. Au(111), 1 MeV.

Since a rosette motion is a typically two-dimensional phenomenon, there is no corresponding one-dimensional motion in the case of planar channeling. Every classical trajectory goes through atomic planes (potential minima) except the unstable case of straight lines going just halfway between atomic planes (potential maxima). Consequently, a transmission maximum cannot be expected *a priori* in a planar case.

On the other hand, a pronounced maximum in transmission has been found in high-energy electron microscopy, when the primary beam is just parallel to a lattice plane, for example, (111) of Au at 1 MeV (Humphreys et al. [20]). This has been interpreted in terms of the usual picture of the dynamical theory, and called the "Bloch-wave channeling" [21]. Thus, the density distribution of the most strongly excited Bloch wave has a large maximum between the atomic planes and, being a symmetric function (corresponding to the 2 s-type), a small maximum at the positions of atomic planes (Figure 8 b). This Bloch wave is obviously weakly absorbed and give rise to an anomalously enhanced transmission.

It was pointed out by Doyle and Berry [22] that this kind of Bloch waves having a large maximum between atomic planes appears every time when the transverse energy (in one dimension) of the Bloch wave is just at the height of the potential maximum between atomic planes (Figure 8 a). This potential maximum may be called the "critical level" of transverse energy. Figure 9 shows schematically the
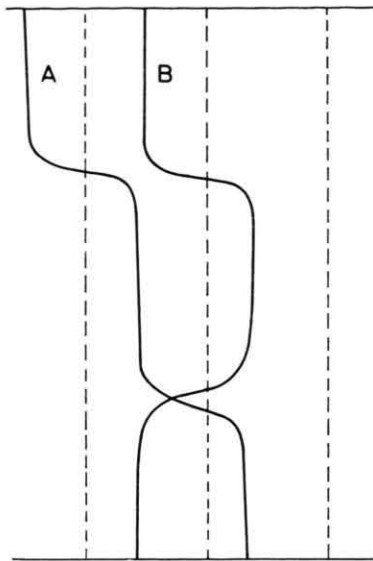
Fig. 9. Planar case. Schematic classical trajectories slightly above (A) and slightly below (B) the critical level of transverse energy.

corresponding classical trajectories at transverse energies slightly above and below the critical level. The paths remain a long time between atomic planes, crossing quickly the atomic planes. It is expected that electrons taking this kind of paths are well transmitted [10]. *We see that the Bloch-wave channeling is essentially not an exclusively wave-mechanical phenomenon, but can be explained equally well by the classical picture.*

If the plane of the drawing of Fig. 9 is assumed to be parallel to a zone axis, the path B is just the picture of a long-wave-length weavon proposed by Nip et al. [6] for explaining an enhanced transmission in axial cases. The path B is then an s-type bound state lying near the critical level. We see in this way that the mechanism of the enhanced transmission for the Bloch-wave channeling is the same as that for the weavons.

Although the above criterion of Doyle and Berry [22] is based on the WKB approach, which is valid only for bound states with higher quantum numbers, it appears to apply satisfactorily also to bound states with low quantum numbers. In fact, the Bloch wave of (111) of Au mentioned above is only the third from the lowest level.

§ 7. Discussion

We could summarize that
1) the most common type of electron channeling is

represented by the deeper lying s-type bound Bloch waves,
2) the rosette motions are the p-type, d-type, etc. bound Bloch waves and
3) the weavons are the s-type bound Bloch waves near the critical level. The Bloch-wave channeling is its special case in the planar channeling.

The type 1) leads always to the increase of Rutherford scattering and the decrease of transmission. Whether the types 2) and 3) lead really to a pronounced increase of transmission and to a decrease of Rutherford scattering depends on the mechanism of inelastic scattering. In the present discussion it was assumed only qualitatively that the concentration of the electron density *at* or *between* the strings leads to an increase or decrease of inelastic scattering. This appears to be sufficient for understanding the essential features of the phenomenon.

We have shown that the concepts in the classical picture of channeling can be applied equally well to the wave-mechanical picture and *vice versa*. Obviously it is only a matter of convenience and accuracy whether we prefer the classical or the wave-mechanical picture. The most important point is to recognize that the channeling as a physical phenomenon of bound states to the atomic strings is present in both regimes.

It is seen that the concept of "bound Bloch waves" of Berry et al. [14] is a powerful tool of interpreting both channeling and diffraction. The semiclassical approach of Berry [14, 15, 16] is naturally a proper way of connecting two phenomena. So far as the wave-mechanical theory is concerned, however, the tight-binding approach appears to be a promising alternative to the usual many-beam approach [19].

Another alternative is, of course, the use of KKR method as proposed by Berry [14]. This method is applicable only in the "muffin-tin model" which may not be always good in the case of continuum potentials. The essential advantage of the KKR method is, however, that one can investigate the bound and free Bloch waves in one formulation. The tight-binding method is appropriate only to bound Bloch waves.

In the present paper we have used the tight-binding theory only for the physical interpretation, but there is a justified hope of using this method also in practical calculations. At higher energies common to channeling experiments the usual many-

beam calculations are suffering from a prohibitingly large number of necessary beams. This problem does not appear in the tight-binding method. The difficulty of calculation is, so to say, shifted to the evaluation of overlap-integrals. The application of the modern techniques of the tight-binding method [19] may improve the situation.

[1] D. S. Gemmell, to be published in Rev. Mod. Physics.
[2] L. T. Chadderton, "Channeling: Theory, Observation and Application", ed. D. V. Morgan, Wiley, London 1973, p. 287.
[3] E. Uggerhøj and F. Frandsen, Phys. Rev. B **2**, 582 [1970].
[4] H. J. Kreiner, F. Bell, R. Sizmann, D. Harder, and W. Hüttl, Phys. Letters **33 A**, 135 [1970].
[5] H. Kumm, F. Bell, R. Sizmann, H. J. Kreiner, and D. Harder, Rad. Effects **12**, 53 [1972].
[6] H. C. H. Nip, M. J. Hollis, and J. C. Kelly, Phys. Letters **28 A**, 324 [1968].
[7] H. C. H. Nip, R. L. Daglish, A. P. M. Chang, and J. C. Kelly, Phys. Letters **34 A**, 257 [1971].
[8] J. Lindhard, Mat. Fys. Medd. Kong. Dan. Vid. Sel. **34**, No. 14 [1965].
[9] F. Fujimoto, S. Takagi, K. Komaki, H. Koike, and Y. Uchida, Rad. Effects **12**, 153 [1972].
[10] F. Fujimoto, K. Komaki, H. Fujita, N. Sumita, Y. Uchida, K. Kambe, and G. Lehmpfuhl, to be published in Proc. of 5th Int. Conf. on Atom. Coll. in Solids, Gatlinburg (Tenn.), USA, Sept. 1973.
[11] A. Ja. Bobudaev, V. V. Kaplin, and S. A. Vorobiev, Phys. Letters **45 A**, 71 [1973].
[12] P. B. Hirsch et al., Electron Microscopy of Thin Crystals, Butterworths, London 1965.
[13] A. Howie, "Modern Diffraction and Imaging Techniques in Material Science", eds. S. Amelinckx et al., North Holland, Amsterdam 1970, p. 295.
[14] M. V. Berry, B. F. Buxton, and A. M. Ozorio de Almeida, **20**, 1 [1970].
[15] M. V. Berry, J. Phys. C **4**, 697 [1971].
[16] M. V. Berry and K. E. Mount, Rep. Progr. Phys. **35**, 315 [1972].
[17] G. Lehmpfuhl, Z. Naturforsch. **28 a**, 1 [1973].
[18] G. Lehmpfuhl, K. Kambe, and F. Fujimoto, to be published.
[19] K. Kambe, to be published.
[20] C. J. Humphreys, L. E. Thomas, J. S. Lally, and R. M. Fisher, Phil. Mag. **23**, 87 [1971].
[21] C. J. Humphreys and J. S. Lally, J. Appl. Phys. **41**, 232 [1970].
[22] P. A. Doyle and M. V. Berry, Z. Naturforsch. **28 a**, 571 [1973].